# Comparison of the Effects of (2*S*,3*S*)-2,3-Methanomethionine, (2*R*,3*R*)-2,3-Methanomethionine, and (2*R*,3*R*)-2,3-Methanophenylalanine on the Conformations of Small Peptides

**Kevin Burgess,* Kwok-Kan Ho, and Biman Pal**

*Contribution from the Department of Chemistry, Texas A&M University, College Station, Texas 77843-3255*

*Received August 10, 1994*[⊗]

**Abstract:** The goal of this paper is to lay foundations for an understanding of the local conformational effects of 2,3-methanoamino acids on secondary structures. These studies are a necessary preliminary to the anticipated applications of 2,3-methanoamino acids in rational manipulation of peptidomimetic and protein-mimic conformations. Details of the research described are as follows. Quenched molecular dynamics (QMD) studies have been performed to compare the conformational effects of (2*S*,3*S*)-2,3-methanomethionine (**2*S*,3*S*-cyclo-M**), (2*R*,3*R*)-2,3-methanomethionine (**2*R*,3*R*-cyclo-M**), and (2*R*,3*R*)-2,3-methanophenylalanine (**2*R*,3*R*-cyclo-F**) incorporated into small peptide systems. Data generated for F{**2*R*,3*R*-cyclo-M**}RF-$NH_2$ and F{**2*S*,3*S*-cyclo-M**}R{**2*R*,3*R*-cyclo-F**}-$NH_2$ were compared with that previously obtained for F{**2*S*,3*S*-cyclo-M**}RF-$NH_2$ (*J. Am. Chem. Soc.* **1995**, *117*, 54). This approach facilitated comparisons between enantiomeric methanoamino acids (**2*S*,3*S*-cyclo-M** and **2*R*,3*R*-cyclo-M** which have the amine and side chain functions *trans*-oriented across a cyclopropane) and between *cis*- and *trans*-2,3-methanoamino acids (*i.e.* **2*R*,3*R*-cyclo-M** and **2*R*,3*R*-cyclo-F**). To effect this comparison, the local influences of the 2,3-methanoamino acids were visualized and rationalized using $\phi,\psi$ dot plots and Newman projections, respectively. For **2*S*,3*S*-cyclo-M**, the $\psi$ constraints caused by the 3-substituent were greater than the corresponding $\phi$ restrictions. The fundamental difference between the enantiomers of (*E*)-2,3-methanomethionine was that $\psi$ values for **2*S*,3*S*-cyclo-M** in the peptidomimetics tended to be more positive than the corresponding torsions for **2*R*,3*R*-cyclo-M**. For the *cis* methanolog, **2*R*,3*R*-cyclo-F**, $\phi$ values were more severely affected than $\psi$ torsions, unlike the situation outlined for the ***E*-cyclo-M** enantiomers. NMR experiments also were performed to determine any conformational biases of F{**2*R*,3*R*-cyclo-M**}RF-$NH_2$ and F{**2*S*,3*S*-cyclo-M**}R{**2*R*,3*R*-cyclo-F**}-$NH_2$ in dimethyl sulfoxide (DMSO) solution. These data were then compared with results from the calculations. Both the NMR and QMD studies indicated that F{**2*S*,3*S*-cyclo-M**}R{**2*R*,3*R*-cyclo-F**}-$NH_2$ had a bias toward a structure with all the side chains oriented on one face of the molecule and all the carbonyl vectors pointing in the opposite direction. Inconsistencies between the NMR and QMD data arose for F{**2*R*,3*R*-cyclo-M**}RF-$NH_2$, *i.e.* conformers fitting the NMR data could be located in the families of structures generated by the QMD experiments, but they did not appear to be the most favorable ones in the theoretical approach. It is suggested that these ambiguities could be due to contributions from different conformers with energies relatively close to the global minimum.

## Introduction

Until recently, the solution conformational effects of peptidomimetics containing 2,3-methanoamino acids,[1] like (2*R*,3*R*)-2,3-methanomethionine (**2*R*,3*R*-cyclo-M**), (2S,3S)-2,3-methanomethionine (**2*S*,3*S*-cyclo-M**), and (2R,3R)-2,3-methanophenylalanine (**2*R*,3*R*-cyclo-F**), were almost completely unexplored. In fact, the state of the field can be summarized very briefly. Theoretical work had indicated that these amino acid surrogates would impose significant conformational constraints,[2-5] crystallographic studies had shown some conformational biases in the solid state,[6-9] and limited NMR/modeling experiments had implied dipeptide analogues of aspartame (Asp-Phe-OMe) could adopt a putative conformation required for sweet taste.[10]

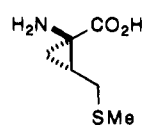


**2*R*,3*R*-cyclo-Met**

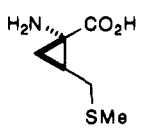


**2*S*,3*S*-cyclo-Met**

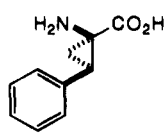


**2*R*,3*R*-cyclo-Phe**

Our group has begun a project to prepare 2,3-methanoamino acids in optically pure form[11-15] and examine the structural and

[⊗] Abstract published in *Advance ACS Abstracts*, March 1, 1995.

(1) Stammer, C. H. *Tetrahedron* **1990**, *46*, 2231.
(2) Barone, V.; Fraternali, F.; Cristinziano, P. L.; Lelj, F.; Rosa, A. *Biopolymers* **1988**, *27*, 1673.
(3) Varughese, K. I.; Srinivasan, A. R.; Stammer, C. H. *Int. J. Pept. Protein Res.* **1985**, *26*, 242.
(4) Varughese, K. I.; Wang, C. H.; Kimura, H.; Stammer, C. H. *Int. J. Pept. Protein Res.* **1988**, *31*, 299.
(5) Taylor, E. W.; Wilson, S.; Stammer, C. H. *ACS Symp. Ser.* **1991**, 162.
(6) Toniolo, C.; Crisma, M.; Valle, G.; Bonora, G. M.; Barone, V.; Benedetti, E.; Blasio, B. D.; Pavone, V.; Pedone, C.; Santini, A.; Lelj, F. *Pept. Chem.* **1987**, 45.
(7) Benedetti, E.; Blasio, B. D.; Pavone, V.; Pedone, C.; Santini, A.; Crisma, M.; Valle, G.; Toniolo, C. *Biopolymers* **1989**, *28*, 175.
(8) Valle, G.; Crisma, M.; Toniolo, C.; Holt, E. M.; Tamura, M.; Bland, J.; Stammer, C. H. *Int. J. Pept. Protein Res.* **1989**, *34*, 56.
(9) Crisma, M.; Bonora, G. M.; Toniolo, C.; Benedetti, E.; Bavoso, A.; Blasio, B. D.; Pavone, V.; Pedone, C. *Int. J. Biol. Macromol.* **1988**, *10*, 200.
(10) Zhu, Y. F.; Yamazaki, T.; Tsang, J. W.; Lok, S.; Goodman, M. *J. Org. Chem.* **1992**, *57*, 1074.
(11) Burgess, K.; Ho, K.-K. *J. Org. Chem.* **1992**, *57*, 5931.
(12) Burgess, K.; Ho, K.-K. *Tetrahedron Lett.* **1992**, *33*, 5677.

0002-7863/95/1517-3808$09.00/0 

biochemical effects of substituting these for natural amino acids in peptides and proteins.[16,17] Preceding papers in this series[18,19] described results that indicate that F{**2S,3S-cyclo-M**}RF-$NH_2$ had a detectable (NMR) bias toward a $\gamma$-turn structure in dimethyl sulfoxide (DMSO), whereas the parent peptide FMRF-$NH_2$ was a random coil in the same solvent.[18]

This paper focuses on the local conformational effects of 2,3-methanoamino acids on peptides. There are four stereoisomeric forms of 3-substituted 2,3-methanoamino acids, and each of them exerts different biases on the structure of a peptide. Two fundamental questions must be answered to understand the preferred secondary structures for 3-substituted 2,3-methanoamino acids. Specifically, what are the differences between the conformational biases imposed by (i) enantiomeric 3-substituted-2,3-methanoamino acids (*e.g.* the two enantiomers of ***E*-cyclo-M**) and (ii) epimeric 3-substituted-2,3-methanoamino acids (*i.e. cis*- and *trans*-3-substituted 2,3-methanoamino acids).

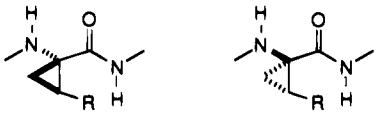

**enantiomeric *trans*-methanologs**

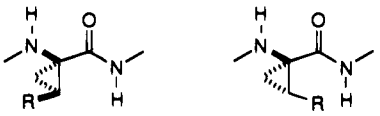

***cis*-** ***trans*-**

**epimeric methanologs**

Consequently, **2*R*,3*R*-cyclo-M**, **2*S*,3*S*-cyclo-M**, and **2*R*,3*R*-cyclo-F** were examined in the context of the peptide that we have been using as a model, FMRF-$NH_2$.

## Experimental Section

**FMOC-2*R*,3*R*-cyclo-F-$NH_2$.** (2*R*,3*R*)-2,3-Methanophenylalanine was prepared as previously described by Davis and Cantrell.[20] Chlorotrimethylsilane (TMSCl, 0.037 g, 0.338 mmol) was added to a vigorously stirred suspension of **2*R*,3*R*-cyclo-F** (0.030 g, 0.169 mmol) in $CH_2Cl_2$ (1.6 mL), and the mixture was refluxed for 1 h. After cooling to 25 °C, the reaction mixture was placed in an ice bath and *N,N*-diisopropylethylamine (0.070 g, 0.541 mmol) was added, followed by (9-fluorenylmethyloxycarbonyl)-*N*-hydroxysuccinimide (FMOC-OSu, 0.063 g, 0.186 mmol). The reaction was allowed to proceed at 0 °C for 20 min, and at 25 °C for 1.5 h. An aqueous solution of 2.5% $NaHCO_3$ (10 mL) was added, and then the aqueous layer was washed with $Et_2O$ (3 × 10 mL). Combined $Et_2O$ layers were back-extracted with $H_2O$ (2 × 10 mL). The $NaHCO_3$ solution and the $H_2O$ extracts were combined, acidified to pH = 2 using 1 M HCl, and extracted with EtOAc (3 × 15 mL). The combined organic layers were dried and evaporated. The residue was purified by flash chromatography (20−40% acetone/hexane, acidified with acetic acid by addition of *ca.* 2 drops of acetic acid/20 mL of eluent) to give **FMOC-{2*R*,3*R*-cyclo-F}** (0.050 g, 73%) as a colorless solid: $R_f$ 0.25 (33% acetone/hexane acidified with acetic acid); $^1$H-NMR (300 MHz, acetone-$d_6$) $\delta$ 7.84 (d, $J$ = 7.44 Hz, 2H), 7.58 (m, 2H), 7.42−7.18 (m, 9H), 6.75 (br s, 1H), 4.21 (m, 2H), 4.07 (m, 1H), 3.04 (t, $J$ = 8.7 Hz, 1H), 2.94 (br s, 1H), 1.96 (m, 1H), 1.81(m, 1H); $[\alpha]^{26}_D$ +35.8° ($c$ = 1.1, DMF).

**F{2*S*,3*S*-cyclo-M}R{2*R*,3*R*-cyclo-F}-$NH_2$.** FMOC-(2*S*,3*S*)-2,3-Methanomethionine was prepared as described in the preceding paper in this series.[19] The peptidomimetic was prepared by stepwise couplings of FMOC-amino acid derivatives on Rink amide resin. The 4-methoxy-2,3,6-trimethylbenzene sulfonyl (Mtr) group was used as side chain protection for arginine (*i.e.* FMOC-R(Mtr) was used). Manual peptide synthesis was carried out in a 30 mL vessel fitted with a coarse glass frit by using a manual wrist action shaker (Burrel, Model 75), and reagents were added manually. All reactions were carried at 25 °C unless otherwise specified. A DMF washing cycle (10 × 1 min, *ca.* 10 mL) was incorporated after each coupling and deprotection.

Rink amide resin (0.098 g of 0.47 mmol $g^{-1}$ capacity) was first swelled in DMF (*ca.* 10 mL) for 45 min, and the FMOC protecting group was removed by shaking the resin with 20% piperidine in DMF (2 times, 3 + 7 min). Coupling of **FMOC-2*R*,3*R*-cyclo-F** (20 mg, 0.050 mmol, 1 equiv relative to the resin) was performed by first premixing the amino acid with NMM (8.2 $\mu$L, 0.075 mmol, 1.5 equiv), HOBt (6.8 mg, 0.050 mmol, 1 equiv), and BOP (22 mg, 0.050 mmol, 1 equiv) in DMF (4 mL), and then the mixture was added to the resin, shaken for 4 h, and washed. The resin was end-capped using acetic anhydride (8.7 $\mu$L) and DMAP (5.62 mg) in DMF (2 mL) for 20 min. The FMOC was removed, and the resin was washed as in the previous step. Six coupling cycles of FMOC-$R^3$(Mtr) (48 mg, 0.138 mmol, 3 equiv), NMM (23 $\mu$L, 0.207 mmol, 4.5 equiv), HOBt (19 mg, 0.138 mmol, 3 equiv), and BOP (61 mg, 0.138 mmol, 3 equiv) in DMF (4 mL) were performed to give a negative ninhydrin test. The FMOC was removed, and the resin was washed. For **FMOC-2*S*,3*S*-cyclo-M**[2] (19 mg, 0.050 mmol), 1.1 equiv was used and the reaction mixture was shaken for 4 h. The resin was then end-capped with acetic anhydride as shown previously, followed by removal of the FMOC. Two coupling cycles of FMOC-$F^1$ (53 mg, 0.138 mmol, 3 equiv) were performed and deprotected by the same procedure as FMOC-$R^3$. The resin was then washed with $CH_2Cl_2$ (10 × 1 min) and dried under vacuum.

Cleavage of the peptide from the resin was effected by the following procedure. The resin was cooled to 0 °C in a round bottom flask with a stir bar, and then a mixture of phenol (0.75 g), 1,2-ethanedithiol (0.25 mL), thioanisole (0.5 mL), deionized water (0.5 mL), and trifluoroacetic acid (10 mL) was precooled to 0 °C and added to the resin. The reaction mixture was removed from the ice bath and stirred at 25 °C for 10 h. The resin was then filtered and washed with trifluoroacetic acid (5 mL) and $CH_2Cl_2$ (15 mL). The filtrate was evaporated to *ca.* 2 mL. Deionized water (20 mL) was added, and the aqueous layer was washed with $Et_2O$ (5 × 10 mL). Crude peptide (52 mg) was obtained after lyophilization of the water layer. The crude peptide was further purified by preparative RP-HPLC (Vydac C18 column, 22 mm × 25 cm, 10 $\mu$m) with a linear gradient obtained by mixing solvent **A** (0.05% TFA in water) and solvent **B** (0.05% TFA in acetonitrile). The gradient was programmed to increase from 5 to 60% B over 40 min with a flow rate of 6 mL $min^{-1}$. The peak with a retention time of 29.04 min was collected and lyophilized. The desired peptide (TFA salt) was obtained as a colorless powder (17 mg, 43%): amino acid analysis (normalized for Phe) Phe 1.00, Arg 1.06; FABMS (glycerol) *m/e* 623.4 $(M + 1)^+$; HR-FABMS (glycerol) *m/e* calcd for $C_{31}H_{43}N_8O_4S$ 623.3128, found 623.3125.

**F{2*R*,3*R*-cyclo-M}RF-$NH_2$.** Rink amide resin (0.17 g of 0.47 mmol $g^{-1}$ capacity) was used. The desired peptide (TFA salt) was obtained as a colorless powder (48 mg, 73%) with a retention time of 26.45 min: amino acid analysis (normalized for Phe) Phe 2.00, Arg 1.15; FABMS (glycerol) *m/e* 611.3 $(M + 1)^+$; HR-FABMS (glycerol) *m/e* calcd for $C_{30}H_{43}N_8O_4S$ $(M + 1)^+$ 611.3124, found 611.3124.

**Computational Studies.** The CHARMM (version 20, version 19 default parameters) modeling package was used for the molecular simulations performed in this work.[21] It was first necessary to

(13) Burgess, K.; Ho, K.-K.; Ke, C.-Y. *J. Org. Chem.* **1993**, *58*, 3767.
(14) Burgess, K.; Lim, D.; Ho, K.-K.; Ke, C.-Y. *J. Org. Chem.* **1994**, *59*, 2179.
(15) Burgess, K.; Ho, K.-K.; Moye-Sherman, D. *SYNLETT* **1994**, 575.
(16) Malin, D. H.; Payza, K.; Lake, J. R.; Corriere, L. S.; Benson, T. M.; Smith, D. A.; Baugher, R. K.; Ho, K.-K.; Burgess, K. *Peptides* **1993**, *14*, 47.
(17) Malin, D. H.; Lake, J. R.; Ho, K.-K.; Corriere, L. S.; Garber, T. M.; Waller, M.; Benson, T.; Smith, D. A.; Luu, T.-A.; Burgess, K. *Peptides* **1993**, *14*, 731.
(18) Burgess, K.; Ho, K.-K.; Pettitt, B. M. *J. Am. Chem. Soc.* **1994**, *116*, 799.
(19) Burgess, K.; Ho, K.-K.; Pettitt, B. M. *J. Am. Chem. Soc.* **1995**, *117*, 54.
(20) Davies, H. M. L.; Cantrell, W. R. *Tetrahedron Lett.* **1991**, *32*, 6509.
(21) Brooks, B.; Bruccoleri, R.; Olafson, H.; States, D.; Swaminathan, S.; Karplus, M. *J. Comput. Chem.* **1983**, *4*, 187.

parameterize the 2,3-methanoamino acids. Data for the parameterization process were obtained from crystallographic data[3,22] and from CHARMM defaults. Specifically, equilibrium bond lengths, bond angles, and improper dihedrals were derived from crystallographic coordinates; force constants, nonbonded parameters, and atomic charges were adapted from the CHARMM defaults for natural amino acids. Cyclopropane carbons were assumed to be the same as quaternary, methylene, and methine carbons already described in the CHARMM 19 carbon types. Extended atom representations of the nonpolar hydrogens were used.

Quenched molecular dynamics simulations were performed using the newly generated parameters for the unusual amino acids (*vide supra*).[23,24] Thus, the two molecules of interest, F{**2*R*,3*R*-cyclo-M**}-RF-$NH_2$ and F{**2*S*,3*S*-cyclo-M**}R{**2*R*,3*R*-cyclo-F**}-$NH_2$, were built in extended conformations with positive charges on the amino terminus and the Arg guanidine side chain. These starting conformers were minimized using 1000 steps of the adopted basis Newton−Raphson method and a dielectric constant of 45 representing DMSO. The minimized structure was then subjected to dynamics simulations. Throughout, the equations of motion were integrated using the Verlet algorithm with a time step of 1 fs, and SHAKE was used to constrain all bond lengths containing polar hydrogens. Each individual peptide was heated to 1000 K over 10 ps by increasing the temperature by 10 K every 0.1 ps. The peptide was equilibrated for 10 ps at 1000 K, during which time a ±13 K temperature constraint was applied to the system. Molecular dynamics production runs were then performed in the microcanonical (NVE) ensemble for a total time of 600 ps. The trajectories were saved every 1 ps, and a total of 600 structures were produced. Each of the structures was thoroughly minimized using 1000 steps of steepest decent (SD) followed by adopted basis Newton−Raphson until a rms energy derivative of ≤0.001 kcal $mol^{-1}$ $Å^{-1}$ was obtained. Histograms of energies *vs* number of structures were plotted for the 600 structures after minimization (Figure 1); Gaussian distributions were obtained with no discrete high- or low-energy extremes.

Structures ≤4 kcal $mol^{-1}$ of the global minimum were selected for further analyses. Previous studies, specifically of tuftsin (Thr-Lys-Pro-Arg) and Met-enkephalin (Tyr-Gly-Gly-Phe-Met), have shown that a 3−7 kcal $mol^{-1}$ energy cutoff was sufficient to select the structures which gave reasonable agreement with the NMR data.[23,24] By analogy, it was assumed here that a 4 kcal $mol^{-1}$ cutoff would select the most relevant structures for NMR comparison. The selected low-energy structures were sorted into families on the basis of the rms deviation of each Cα-*C*O fragment. Structures with rms deviation ≤0.6 Å were grouped in the same families. Throughout this study, the family with the lowest-energy conformer detected was denoted F1, and subsequent families were numbered according to the energies of their lowest-energy structures (*i.e.* the family with the lowest-energy structure was F1, the family {excluding F1} with the next lowest-energy structure was F2, *etc.*). The coordinates of the lowest-energy structures of each family were extracted, and protons were built on the heavy atoms using standard geometry. Finally, the interproton distances were calculated from these coordinates for comparisons of the simulated structures with the ROE data obtained in the NMR studies.

**NMR Studies.** NMR spectra were recorded on a Varian XL-400 spectrometer (400 MHz). The peptide/peptidomimetic (10 mM) was dissolved in DMSO-$d_6$ (*d*, 99.9%, Cambridge Isotope Laboratories, distilled from $CaSO_4$ before use). DMSO-$d_6$ ($\delta$ = 2.49 ppm) was used as an internal reference. One-dimensional (1D) $^1$H-NMR spectra were recorded with a spectral width of 5299.4 Hz, 52 992 data points, 128 transients, and a 5 s acquisition time. Vicinal coupling constants were measured from the 1D spectra at ambient temperature. Chemical shifts of the amide and α protons were monitored in the concentration range of 2.0−10.0 mM. The near constant values ($\Delta\delta \leq 0.04$ ppm) indicated no significant aggregation had occurred in the 10 mM solutions. Temperature coefficients of amide protons were measured *via* several

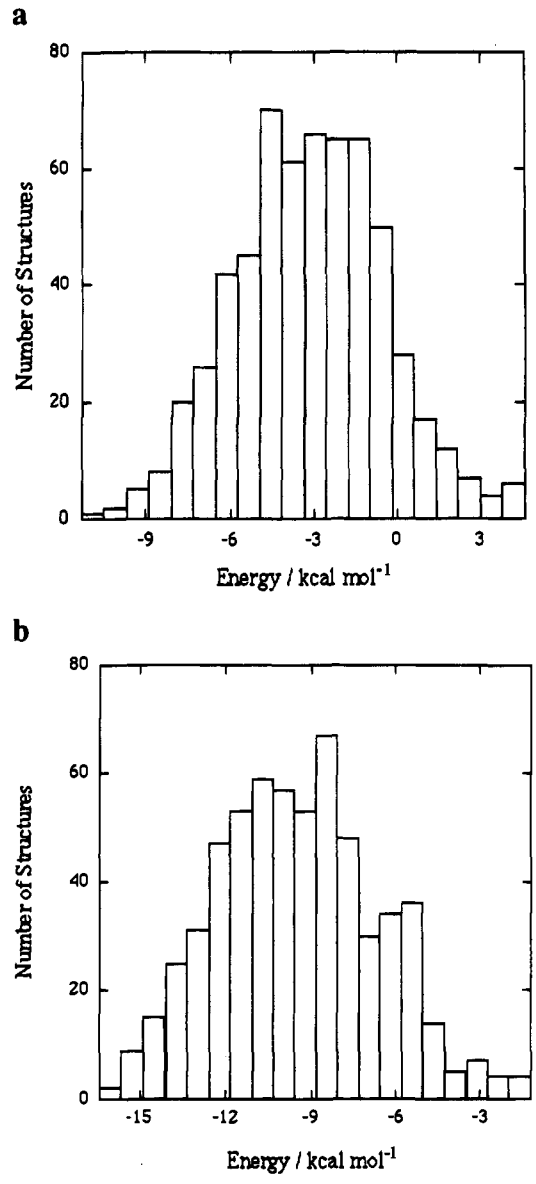


**Figure 1.** Gaussian energy histograms for the QMD study of (a) F{**2*S*,3*S*-cyclo-M**}R{**2*R*,3*R*-cyclo-F**}-$NH_2$ and (b) F{**2*R*,3*R*-cyclo-M**}RF-$NH_2$.

1D experiments from 25 to 65 °C, adjusted in 10 °C increments with equilibration time of ≥8 min after successive temperature steps.

Two-dimensional (2D) spectra were taken at ambient temperature with a spectral width of 5299.4 Hz. Through-bond connectivities were elucidated by DQF-COSY spectra,[25,26] which were recorded with 3 s relaxation delay, 512 $t_1$ increments, and 16 scans per $t_1$ increments with 2 K data points at $t_2$.

Sequential assignments and proton−proton close contacts were elucidated by ROESY spectra (absorption mode),[26,27] which were recorded with a 2 s relaxation delay, 512 $t_1$ increments, and 32 scans per $t_1$ increments with 2 K data points at $t_2$. The spin−lock field was generated by a train of 30° pulses with a resulting spin−lock field strength of 2.0 kHz.[28] The carrier frequency was varied to eliminate COSY, HOHAHA, and "false" NOE artifacts.[29,30] ROESY experiments

(22) Baldwin, J. E.; Adlington, R. M.; Rawlings, B. J.; Jones, R. H. *Tetrahedron Lett.* **1985**, *26*, 485.
(23) O'Connor, S. D.; Smith, P. E.; Al-Obeidi, F.; Pettitt, B. M. *J. Med. Chem.* **1992**, *35*, 2870.
(24) Pettitt, B. M.; Matsunaga, T.; Al-Obeidi, F.; Gehrig, C.; Hruby, V. J.; Karplus, M. *Biophys. J. Biophys. Soc.* **1991**, *60*, 1540.
(25) Piantini, U.; Sorensen, O. W.; Ernst, R. R. *J. Am. Chem. Soc.* **1982**, *104*, 6800.
(26) Wüthrich, K. In *NMR of Proteins and Nucleic Acids*; Wiley: New York, 1986.
(27) Bothner-By, A. A.; Stephen, R. L.; Lee, J.; Warren, C. D.; Jeanloz, R. W. *J. Am. Chem. Soc.* **1984**, *106*, 811.
(28) Kessler, H.; Griesinger, C.; Kerssebaum, R.; Wagner, K.; Ernst, R. R. *J. Am. Chem. Soc.* **1987**, *109*, 607.
(29) Bax, A.; Davis, D. G. *J. Magn. Reson.* **1985**, *63*, 207.
(30) Neuhaus, D. *J. Magn. Reson.* **1986**, *68*, 568.

with mixing times of 75, 150, and 300 ms were recorded to identify peaks caused by spin diffusion.[31] Both DQF-COSY and ROESY data were zero-filled to 2K × 2K data sets, Gaussian transformed in both dimensions, and symmetrized. The intensities of ROESY cross-peaks were assigned as VS (very strong, >4 contours), S (strong, 4 contours), M (medium, 3 contours), W (weak, 2 contours), and VW (very weak, 1 contour) by counting the number of contours. Cutoff distances from ROE data tend to be less than in the corresponding NOE experiments.[32] Nevertheless, an upper level constraint of 5 Å is maintained in this study to ensure that the boundary conditions for comparisons of NMR and experimental data are not too severe.

## Results and Discussion

**Local Effects of the 2,3-Methanoamino Acids on Conformation.** Collected data for the 600 high-energy conformers generated in the QMD studies are shown in Figures 2 and 3 for F{**2*S*,3*S*-cyclo-M**}R{**2*R*,3*R*-cyclo-F**}-$NH_2$ and F{**2*R*,3*R*-cyclo-M**}RF-$NH_2$, respectively.

Distributions of $\phi$ torsions for the natural amino acids in F{**2*S*,3*S*-cyclo-M**}R{**2*R*,3*R*-cyclo-F**}-$NH_2$ and in F{**2*R*,3*R*-cyclo-M**}RF-$NH_2$ were heavily biased toward negative values (Figures 2b and 3b). This reflects the intrinsic steric effects imposed by the $C^{\alpha}$ chiral center of natural amino acids, as can be seen from the Newman projections shown below.

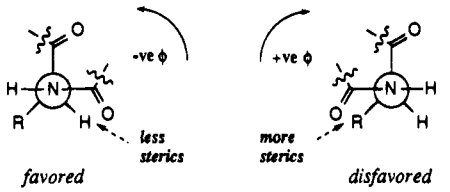


In contrast to the natural amino acids, both negative and positive $\phi$ regions were nearly equally populated for the ***E*-cyclo-M²** derivatives (Figures 2a and 3a). This observation can be rationalized using Newman projections. The only difference between the two Cα side chain substituents of a 3-substituted-2,3-methanoamino acid is the 3-substituent. This substituent is rigidly oriented away from the N−Cα bond in *trans*-cyclopropane amino acids; hence, it has insignificant steric effects on the $\phi$ torsion, as shown below. Moreover, there is

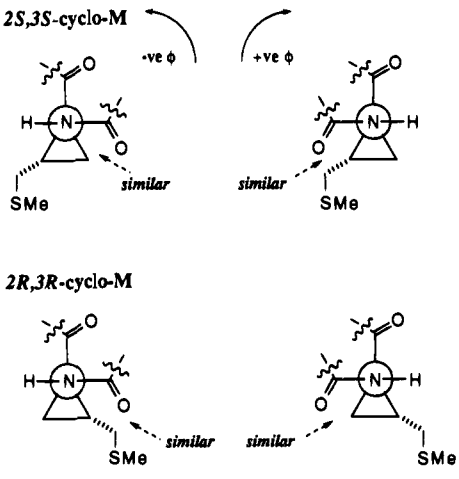


very little difference in the $\phi$ dimension for **2*S*,3*S*-** and **2*R*,3*R*-cyclo-M** because the substituent is held away from the relevant bond rotation for both derivatives.

(31) Kumar, A.; Wagner, G.; Ernst, R. R.; Wüthrich, K. *J. Am. Chem. Soc.* **1981**, *103*, 3654.

(32) Bauer, C. J.; Frenkiel, T. A.; Lane, A. N. *J. Magn. Reson.* **1990**, *87*, 144.

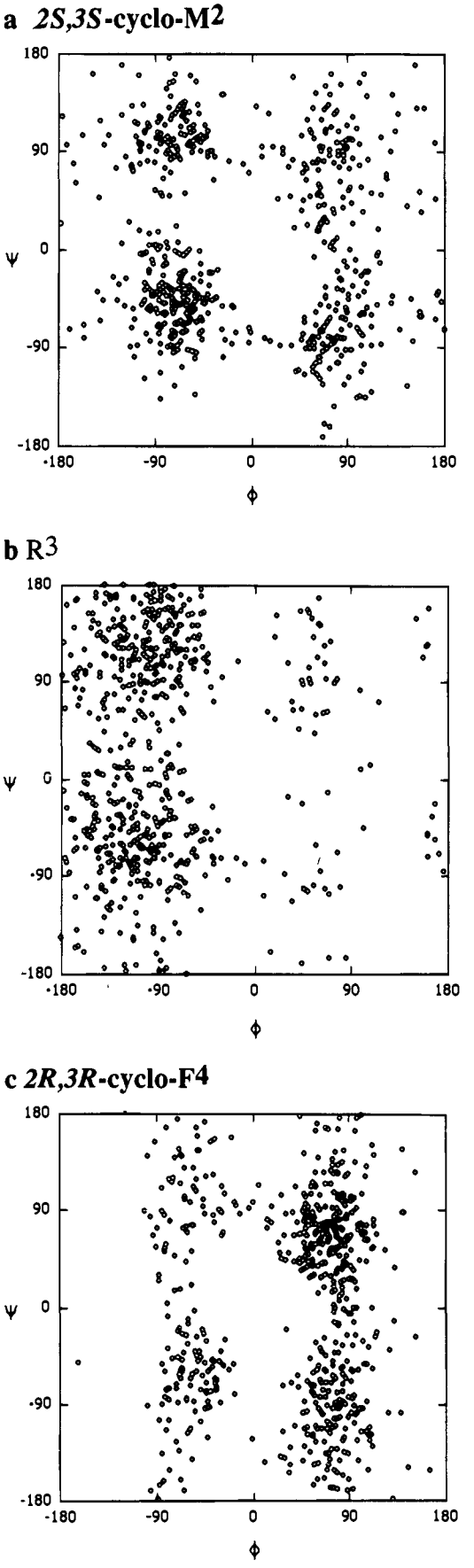


**Figure 2.** $\phi,\psi$ Scatter plots for the amino acid residues of F{**2*S*,3*S*-cyclo-M**}R{**2*R*,3*R*-cyclo-F**}-$NH_2$ at 1000 K after molecular dynamics.

Differences between **2*S*,3*S*-cyclo-M** and **2*R*,3*R*-cyclo-M** are most pronounced in the $\psi$ dimension. Comparison of the relevant scatter plots, Figures 2a and 3a respectively, reveals

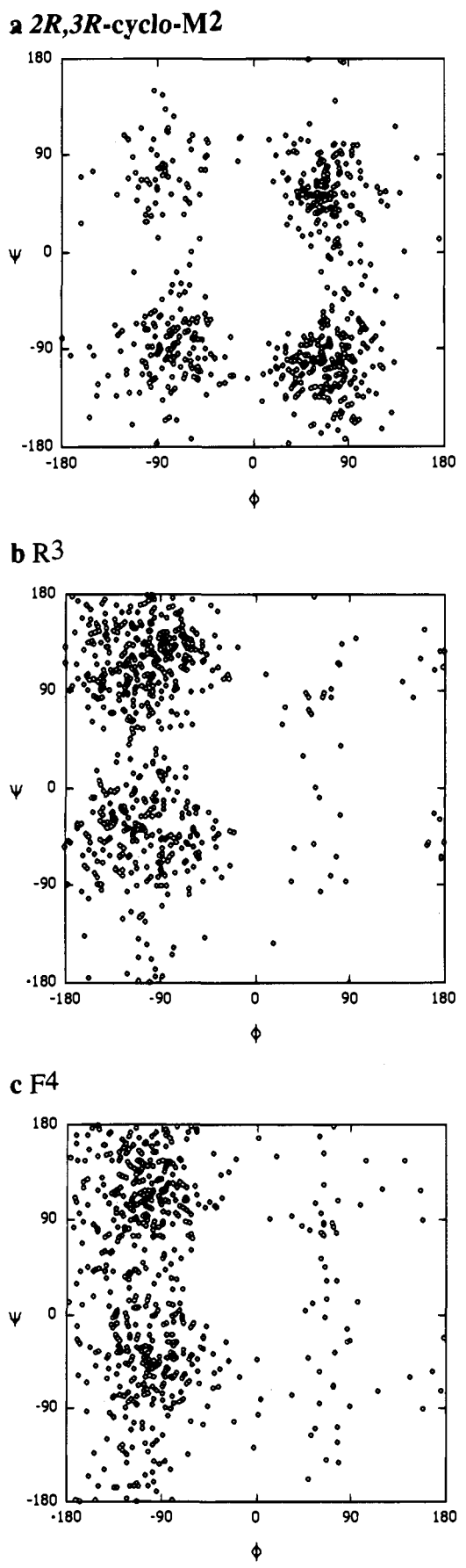


**Figure 3.** $\phi,\psi$ Scatter plots for F{**2*R*,3*R*-cyclo-M**}RF-$NH_2$ at 1000 K after molecular dynamics.

that $\psi$ values for the former amino acid are more positive (or less negative) than the corresponding torsions for the latter stereoisomer. This is consistent with the following reasoning from Newman projections. For **2*S*,3*S*-cyclo-M**, interactions of the cyclopropane 3-substituent with either the peptide fragment on the *C*-terminus (for negative $\psi$ torsions) or the carbonyl oxygen (for positive $\psi$ torsions) are critical. These interactions tend to compress negative $\psi$ angles and expand positive $\psi$ values. Exactly the inverse of this situation applies to **2*R*,3*R*-cyclo-M**, for which negative $\psi$ torsions are expanded and positive ones are compressed, as shown below.

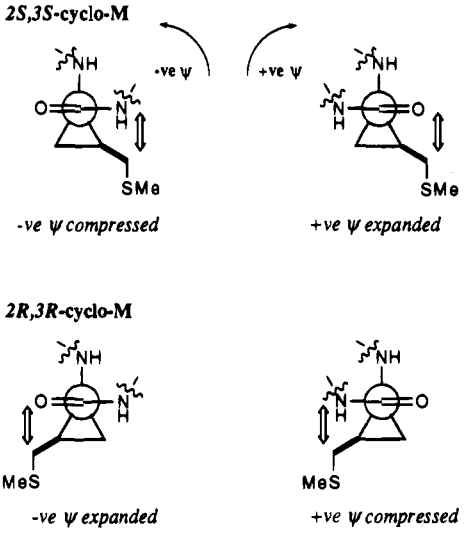


General differences between *E*- and *Z*-methanologs were most pronounced in the $\phi$ dimension, as revealed by comparing **2*R*,3*R*-cyclo-F** and **2*R*,3*R*-cyclo-M** (Figures 2c and 3a). For

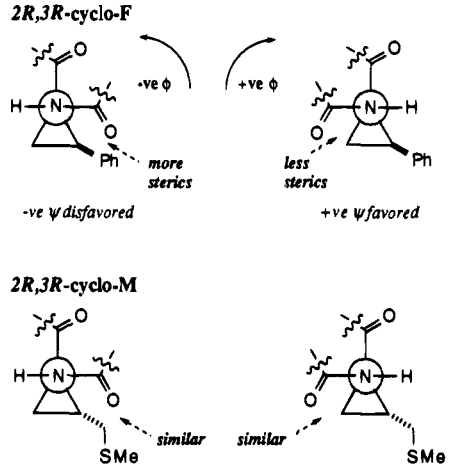


the former, the negative $\phi$ region was relatively underpopulated, presumably because the 3-substituent (*i.e.* the aromatic ring) disfavors rotation about the $\phi$ torsion to that area of conformational space. Conversely, the positive and negative $\phi$ dimensions were almost equally populated for **2*R*,3*R*-cyclo-M** because the 3-substituent of this methanolog is oriented away from the $\phi$ torsion (*vide supra*).

In the $\psi$ dimension, the differences between the *E*- and *Z*-methanologs were small but conspicuous. Comparison of Figures 2c and 3a shows a small but obvious tendency for the positive $\psi$ region of conformational space of the *Z*-methanolog **2*R*,3*R*-cyclo-F** to be more highly populated, and at higher positive $\psi$ values, than the corresponding region in the plot for **2*R*,3*R*-cyclo-M**. This tendency of $\psi$ angles for **2*R*,3*R*-cyclo-M** to be more negative (or less positive) than for **2*R*,3*R*-cyclo-F** is analogous to that which was observed when comparing **2*S*,3*S*-**

**cyclo-M** and **2*R*,3*R*-cyclo-M** (*vide supra*) and is evident from the following projections. The 3-substituent of **2*R*,3*R*-cyclo-F**

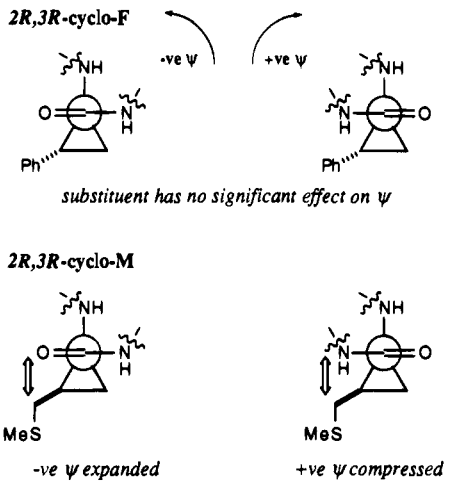


does not exert any effect on the corresponding $\psi$ torsion, whereas for **2*R*,3*R*-cyclo-M**, the substituent causes $\psi$ to tend to expand in the negative direction and contract in the positive one.

Scatter plots for the 600 structures after molecular mechanics minimizations were also informative. Figures 4 and 5 show these plots for F{**2*S*,3*S*-cyclo-M**}R{**2*R*,3*R*-cyclo-F**}-$NH_2$ and F{**2*R*,3*R*-cyclo-M**}RF-$NH_2$, respectively. Distribution of the natural amino acid (*e.g.* $R^3$) conformers converges, as expected, to areas including $\phi,\psi$ torsion regions of most of the common elements of secondary structure (*i.e.* α-helices, turn regions, β-sheets). Thus, the torsions concentrate in the negative $\phi$ region (*vide supra*) and in $\psi$ regions between approximately −70 and −180°. The $\phi,\psi$ scatter plots sampled most of the conformational space available for natural amino acids and resembled the $\phi,\psi$ distribution plot obtained from high-resolution X-ray crystallography of proteins.[33] Successful sampling of the favorable $\phi,\psi$ conformational space by the scatter plots for the natural amino acids implies that $\phi,\psi$ distribution plots for 2,3-methanoamino acids should give reasonable predictions of the available conformational space for these protein amino acid analogs.

The $\phi,\psi$ scatter plots for **2*S*,3*S*-cyclo-M** (Figure 4a), **2*R*,3*R*-cyclo-F** (Figure 4c), and **2*R*,3*R*-cyclo-M** (Figure 5a) after quenching by molecular mechanics minimization show that the populated conformational space was separated into four major regions. The $\phi$ torsions took very narrow values centered at +70 or −70°. A very significant bias toward positive $\phi$ torsions was observed for **2*R*,3*R*-cyclo-F** as compared with **2*S*,3*S*-cyclo-M**; this is the same trend followed for the high-energy conformations before minimization. Nevertheless, the areas of conformational space that were populated for both residues covered the γ-turn, inverse-γ-turn, $\alpha_R$-helix, and $\alpha_L$-helix regions. A $3_{10}$-helical conformation (*ca.* $\phi,\psi$ −50, −30°) was accessible to **2*S*,3*S*-cyclo-M** and marginally so for **2*R*,3*R*-cyclo-F**. However, the data described above indicate that $3_{10}$-helical conformations are not favorable for **2*R*,3*R*-cyclo-M**, at least not in the peptidomimetics studied here.

**Calculated Influences of the 2,3-Methanoamino Acids on Overall Peptide Conformations.** The low-energy structures of F{**2*S*,3*S*-cyclo-M**}R{**2*R*,3*R*-cyclo-F**}-$NH_2$ (*i.e.* within 4 kcal $mol^{-1}$ of the minimum-energy conformer overall) were sorted into four families with a total of 36 structures. Two major families, F1 and F2, had 8 and 19 members, respectively (Table

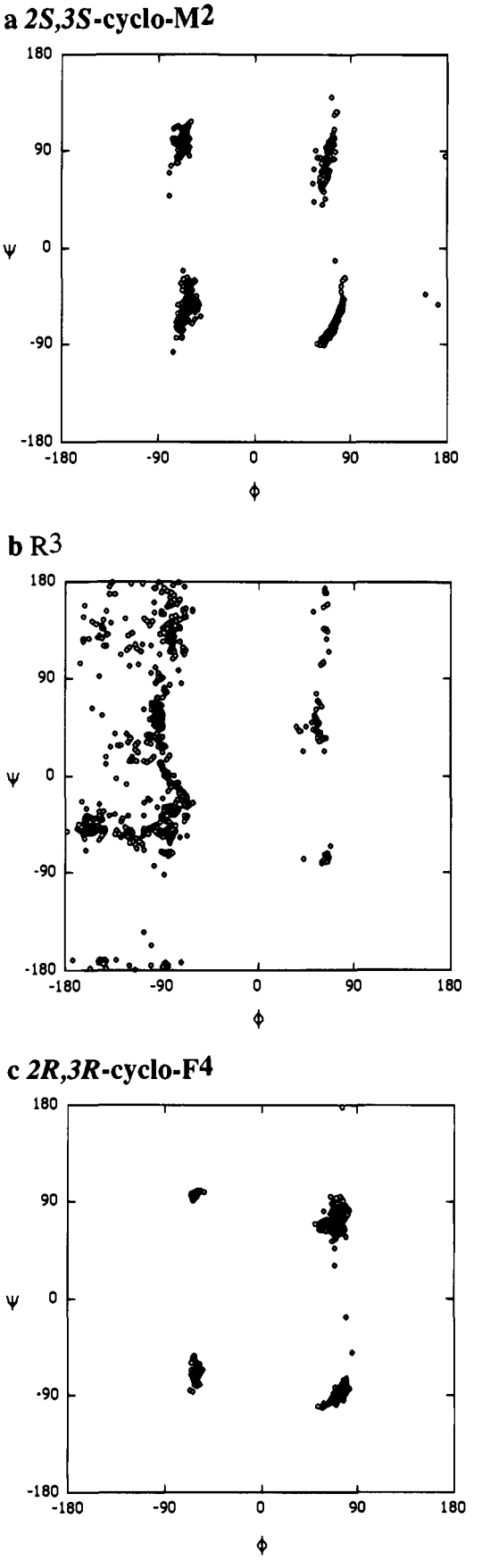


**Figure 4.** $\phi,\psi$ Scatter plots for the 600 conformers of F{**2*S*,3*S*-cyclo-M**}R{**2*R*,3*R*-cyclo-F**}-$NH_2$ after quenching *via* molecular mechanics minimizations.

(33) Richardson, J. S. In *Advances in Protein Chemistry*; Anfinsen, C. B., Edsall, J. J., Richards, F. M., Eds.; Academic Press: New York, 1981; Vol. 34, p 167.

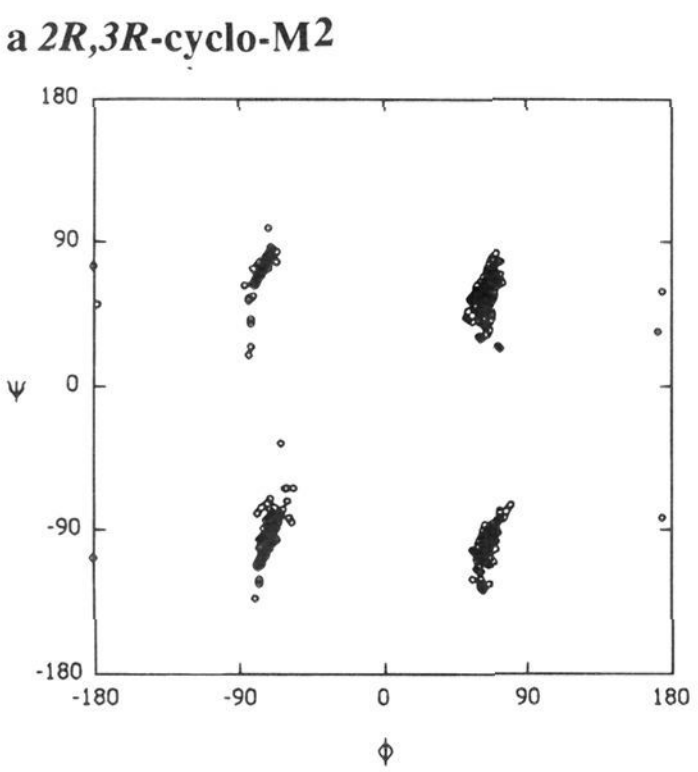


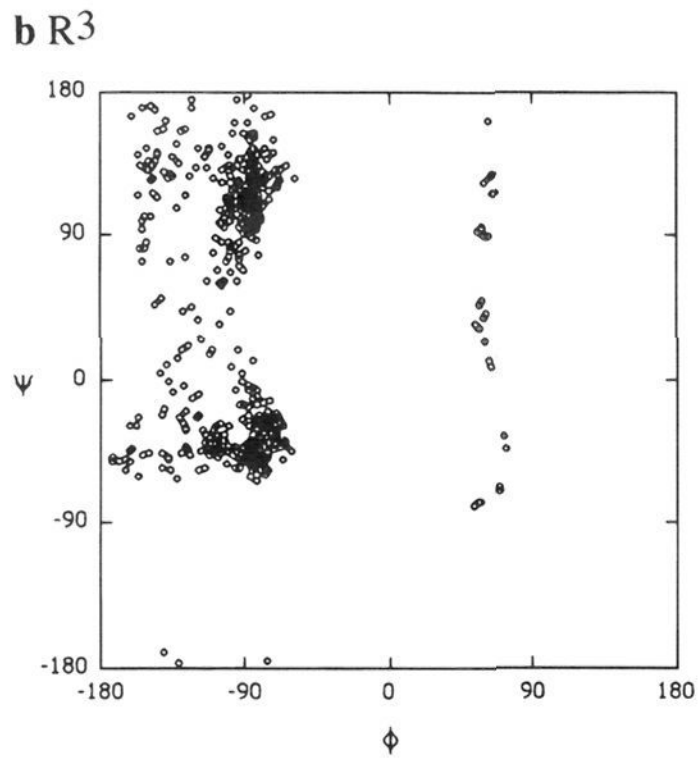


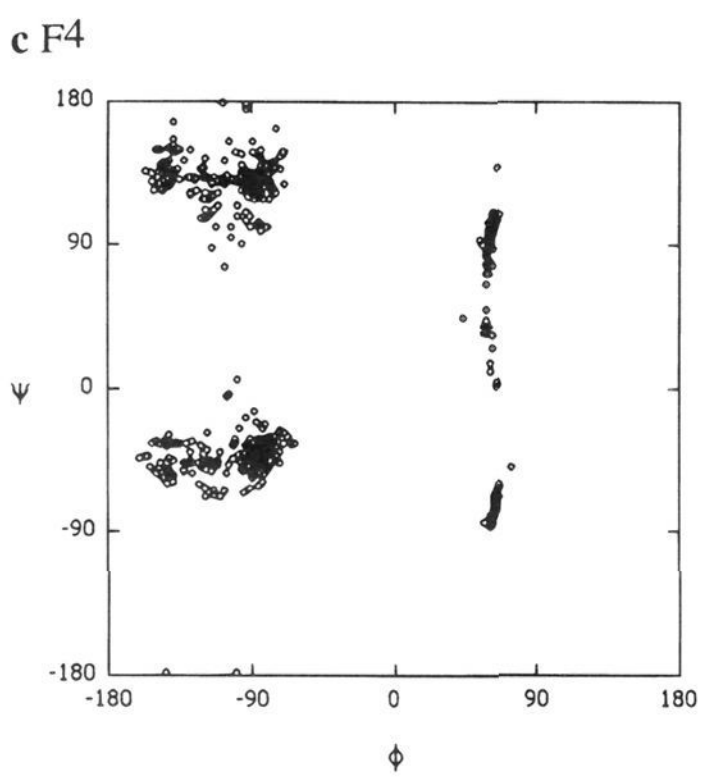


**Figure 5.** $\phi,\psi$ Scatter plots for the 600 conformers of F{***2R,3R*-cyclo-M**}RF-$NH_2$ after quenching *via* molecular mechanics minimizations.

**Table 1.** Structural Characteristics of Typical Low-Energy Conformers from Each of the Families Generated in the QMD Study of F{**2*S*,3*S*-cyclo-M**}R{**2*R*,3*R*-cyclo-F**}-$NH_2$

| residue | dihedral angle | F1 | F2 | F3 | F4 |
|---|---|---|---|---|---|
| $F^1$ | $\psi$ | 151 | 114 | −54 | −29 |
| | $\chi_1$ | −173 | −162 | −175 | 68 |
| | $\chi_2$ | 60 | 85 | 52 | −71 |
| **2*S*,3*S*-cyclo-M$^2$** | $\phi$ | −56 | −63 | 81 | 73 |
| | $\psi$ | −54 | −34 | −34 | −78 |
| | $\chi_1$ | 151 | 151 | 157 | 150 |
| | $\chi_2$ | −64 | −178 | −68 | 62 |
| $R^3$ | $\phi$ | −78 | −89 | −70 | −141 |
| | $\psi$ | −36 | 22 | −28 | 120 |
| | $\chi_1$ | −67 | −67 | −51 | −168 |
| | $\chi_2$ | 179 | 67 | −58 | 73 |
| **2*R*,3*R*-cyclo-F$^4$** | $\phi$ | −61 | 78 | 74 | 69 |
| | $\psi$ | −67 | −85 | 80 | 83 |
| | $\chi_1$ | −4 | −3 | −3 | −5 |
| | $\chi_2$ | −92 | 78 | 100 | −84 |
| number of members in family | | 8 | 19 | 4 | 2 |
| lowest energy (kcal $mol^{-1}$) | | −11.2 | −9.9 | −8.5 | −8.2 |

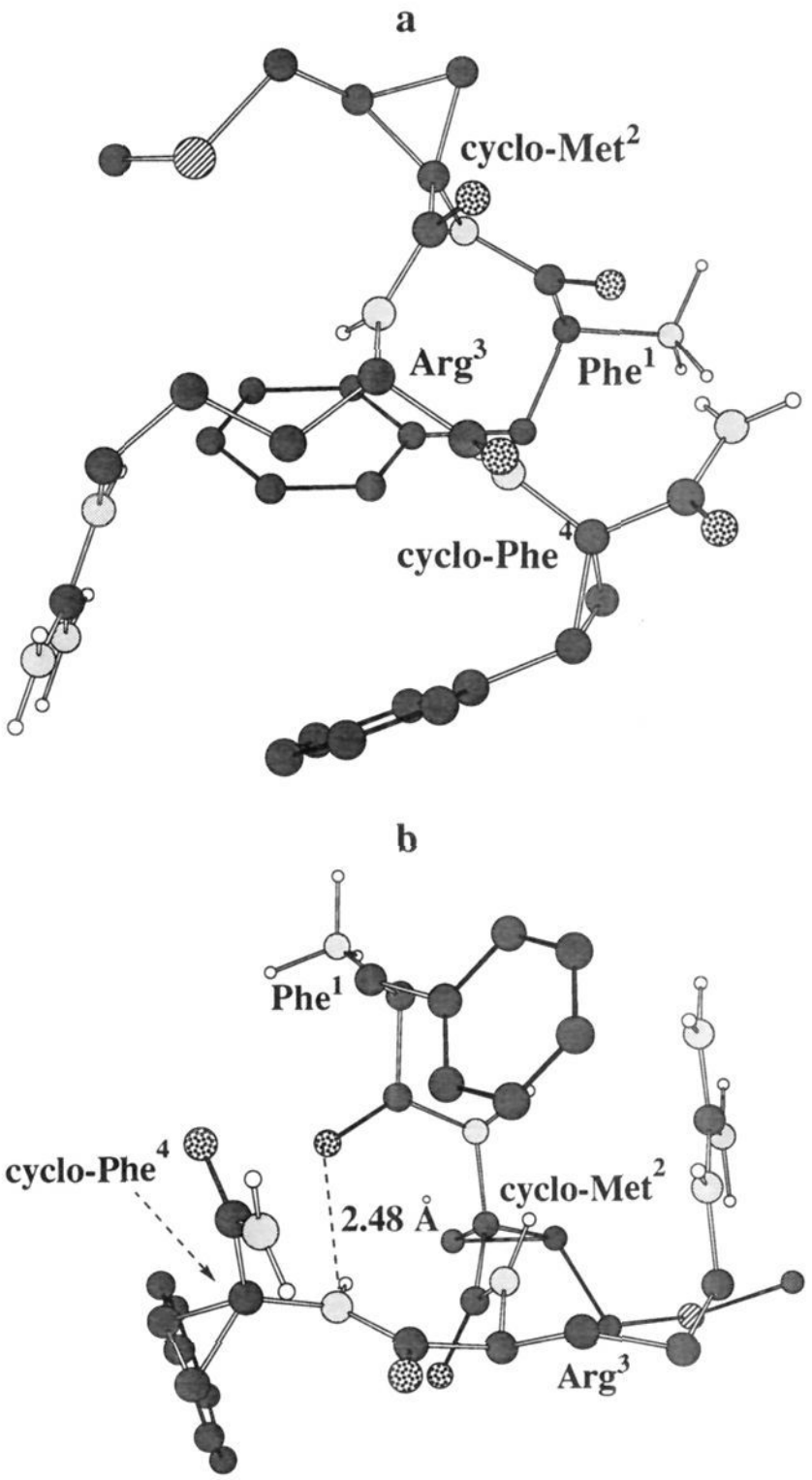


**Figure 6.** Lowest-energy structures of families F1 (a) and F2 (b) for F{***2S,3S*-cyclo-M**}R{***2R,3R*-cyclo-F**}-$NH_2$. The latter shows a type I $\beta$-turn structure.

1). The lowest-energy structure (in family F1 by definition, Figure 6a) had no hydrogen bond, and all of the side chains and N*H* vectors were oriented in one direction, while all the carbonyl groups were pointing in the opposite direction. The lowest-energy structure of family F2 had one hydrogen bond between the $F^4NH$ and the $F^1CO$, giving a type I $\beta$-turn structure

**Table 2.** Structural Characteristics of Typical Low-Energy Conformers from Each of the Families Generated in the QMD Study of F{**2*R*,3*R*-cyclo-M**}RF-$NH_2$

| residue | dihedral angle | F1 | F2 | F3 | F4 | F5 | F6 |
|---|---|---|---|---|---|---|---|
| $F^1$ | $\psi$ | 136 | 141 | −56 | 144 | −58 | −86 |
| | $\chi_1$ | 64 | −62 | −171 | −178 | −175 | −178 |
| | $\chi_2$ | −71 | 93 | −94 | 64 | 58 | 62 |
| **2*R*,3*R*-cyclo-M²** | $\phi$ | 63 | −77 | 67 | −70 | 67 | 53 |
| | $\psi$ | −91 | 68 | −94 | 81 | −90 | 46 |
| | $\chi_1$ | −153 | −152 | −153 | −154 | −153 | −150 |
| | $\chi_2$ | 179 | 178 | 67 | 178 | 177 | 64 |
| $R^3$ | $\phi$ | −74 | −155 | −135 | −85 | −70 | −115 |
| | $\psi$ | −26 | −24 | −8 | 109 | 122 | −56 |
| | $\chi_1$ | 66 | 57 | 61 | −63 | −174 | −79 |
| | $\chi_2$ | −122 | −177 | −161 | 171 | 70 | −67 |
| $F^4$ | $\phi$ | −88 | −81 | −90 | −93 | −83 | −124 |
| | $\psi$ | 124 | 127 | −56 | −45 | 118 | 123 |
| | $\chi_1$ | −54 | −57 | −50 | −60 | −55 | −58 |
| | $\chi_2$ | −60 | −61 | −78 | 111 | −74 | 110 |
| number of members in family | | 29 | 4 | 28 | 7 | 7 | 7 |
| lowest energy (kcal $mol^{-1}$) | | −16.4 | −15.4 | −15.0 | −14.9 | −14.6 | −14.3 |

(Figure 6b). Four minor families were also obtained with 1−4 members, and the characteristics of the more populated ones (F3 and F4) are shown in Table 1. However, these families were relatively insignificant because they were less populated than the major ones and because the lowest-energy conformer that they contained was significantly higher in energy than the corresponding low-energy structures for F1 and F2.

The QMD study of F{**2*R*,3*R*-cyclo-M**}RF-$NH_2$ gave two major families (Table 2). There were 91 conformers within 4 kcal $mol^{-1}$ of the lowest-energy structure overall in this particular QMD experiment, and 29 of them were grouped in the same family as this low-energy structure. This structure was stabilized by two hydrogen bonds (Figure 7a): one between $F^4NH$ and $F^1CO$ forming a 10-member ring and the other between $F^1NH$ and $F^4CO$. The $\phi,\psi$ torsions of the **2*R*,3*R*-cyclo-M²** and $R^3$ residues were 63, −91° and −74, −26° respectively, which are reasonably close to the expected values for $i + 1$ and $i + 2$ residues in a type II′ $\beta$-turn structure.[34] The other major family (F3) contains 28 members. In the lowest-energy conformer from this family, a hydrogen bond between the $F^4NH$ and the $F^1CO$ rendered it very similar to a type II′ $\beta$-turn (Figure 7b). For the minor families F2 (4 members) and F4 (7 members), the low-energy conformers were inverse $\gamma$-turn structures centered at the **2*R*,3*R*-cyclo-M²** (*i.e.* hydrogen bond between $R^3NH$ and the $F^1CO$) while a $\gamma$-turn structure was the minimum in F5 (7 members).

**NMR Studies of F{2*S*,3*S*-cyclo-M}R{2*R*,3*R*-cyclo-F}-$NH_2$ and F{2*R*,3*R*-cyclo-M}RF-$NH_2$.** Chemical shift assignments for F{**2*S*,3*S*-cyclo-M**}R{**2*R*,3*R*-cyclo-F**}-$NH_2$ and for F{**2*R*,3*R*-cyclo-M**}RF-$NH_2$ in DMSO were made by tracing COSY and ROESY connectivities in the usual manner,[26] and the chemical shift assignments are presented in Table 3. For F{**2*S*,3*S*-cyclo-M**}R{**2*R*,3*R*-cyclo-F**}-$NH_2$, all the amide proton temperature coefficients were above −3.00 ppb $K^{-1}$, and no striking trends could be deduced from the chemical shift information.

Replacement of two natural amino acids with the two 2,3-methanoamino acids in F{**2*S*,3*S*-cyclo-M**}R{**2*R*,3*R*-cyclo-F**}-$NH_2$ had a drastic line-broadening effect on some $^1$H-NMR signals. This is shown in Figure 8 which displays spectra of the parent peptide FMRF-$NH_2$ and of F{**2*S*,3*S*-cyclo-M**}R-{**2*R*,3*R*-cyclo-F**}-$NH_2$. Thus, a doublet $R^3NH$ signal was observed for FMRF-$NH_2$, whereas the corresponding signal for F{**2*S*,3*S*-cyclo-M**}R{**2*R*,3*R*-cyclo-F**}-$NH_2$ was a broad singlet.

(34) Rose, G. D.; Gierasch, L. M.; Smith, J. A. In *Advances in Protein Chemistry: Turns in Peptides and Proteins*; Academic Press, Inc.: New York, 1985.

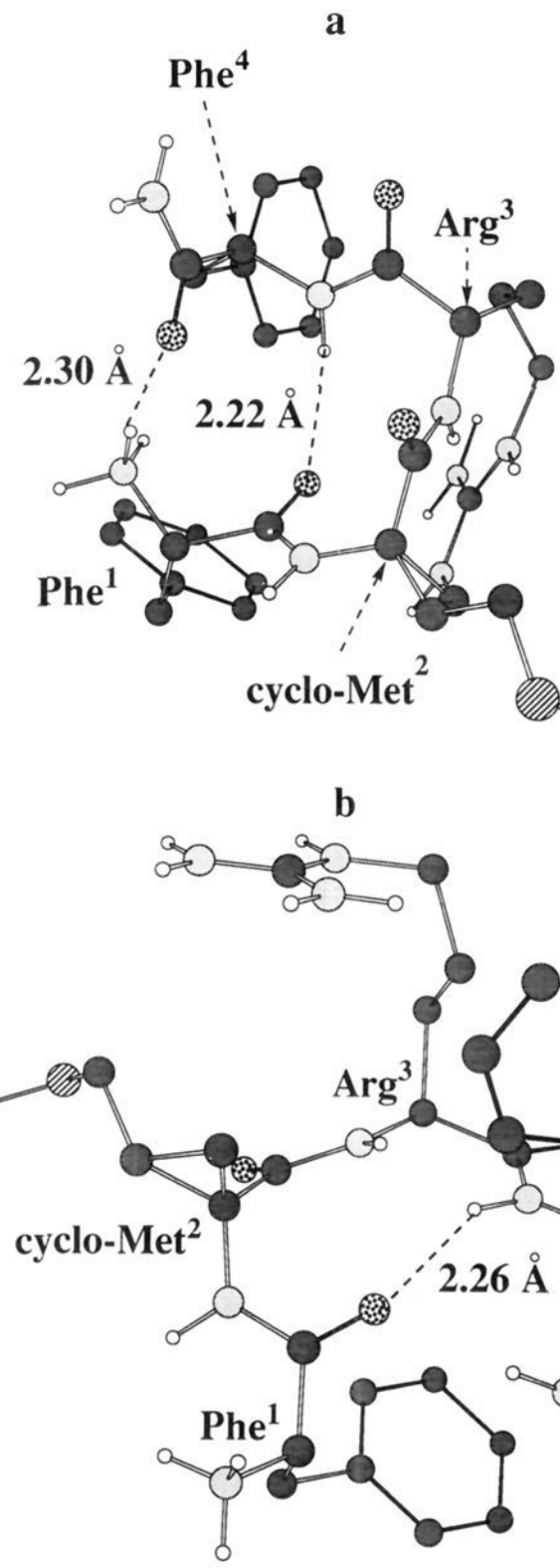


**Figure 7.** (a) Minimum-energy conformer overall (family F1) for F{**2*R*,3*R*-cyclo-M**}RF-$NH_2$. This structure is a type II′ $\beta$-turn. (b) The low-energy conformer from family F3 in the QMD study of F{**2*R*,-3*R*-cyclo-M**}RF-$NH_2$ has a structure very similar to a type II′ $\beta$-turn.

Similar effects were observed for the $F^1\alpha$ and $R^3\alpha$ protons. Overall, this line broadening suggests that F{**2*S*,3*S*-cyclo-M**}R-

**Table 3.** Chemical Shifts, Coupling Constants, and Temperature Coefficients of Various Protons in $FX^2RX^4$-$NH_2$

| | | δ (ppm) {important coupling (Hz)} [temperature coefficient (ppb $K^{-1}$)] | |
|---|---|---|---|
| acid | proton | $X^2$ = 2*S*,3*S*-cyclo-M $X^4$ = 2*R*,3*R*-cyclo-F | $X^4$ = 2*R*,3*R*-cyclo-M |
| $F^1$ | NH | 8.23 {br singlet} | 8.29 {br singlet} |
| | α | 3.96 | 3.93 |
| | β | 3.14 | 3.30 {Jα-β, 6.8} |
| | β | 2.95 | 2.88 {Jα-β, 8.8} |
| $X^2$ | NH | 9.09 {br singlet} [−3.80] | 8.91 {singlet} [−2.18] |
| | α | – | – |
| | β | 1.34 | 1.10 |
| | β | – | – |
| | β′ | 1.34[a] | 1.31 (*trans*) |
| | β′ | 0.85[a] | 0.50 (*cis*) |
| | γ | 2.63 | 2.45 |
| | γ | 2.52 | 2.45 |
| | ϵ | 2.02 | 1.86 |
| $R^3$ | NH | 7.77 {br singlet} [-6.10] | 7.57 {JNH-α, 8.4} [−2.80] |
| | α | 3.82 | 4.35 |
| | β | 1.34 | 1.62 |
| | β | 1.34 | 1.52 |
| | γ | 1.08 | 1.39 |
| | γ | 1.08 | 1.39 |
| | δ | 2.88 | 3.04 |
| | δ | 2.88 | 3.04 |
| | NHϵ | 7.54 | 7.53 |
| $X^4$ | NH | 7.95 {singlet} [−5.40] | 7.99 {JNH-α, 8.0} [−5.09] |
| | α | – | 4.41 |
| | β | 2.78 | 2.95 {Jα-β, 5.2} |
| | β | – | 2.80 {Jα-β, 8.8} |
| | $\beta'_{trans}$[b] | 1.71 | |
| | $\beta'_{cis}$[b] | 1.56 | |

[a] The β′ protons are those of the cyclopropane methylene group. Stereospecific assignment was not possible due to overlapping of β and β′ protons (1.34 ppm). [b] *Cis* or *trans* to the amino terminus.

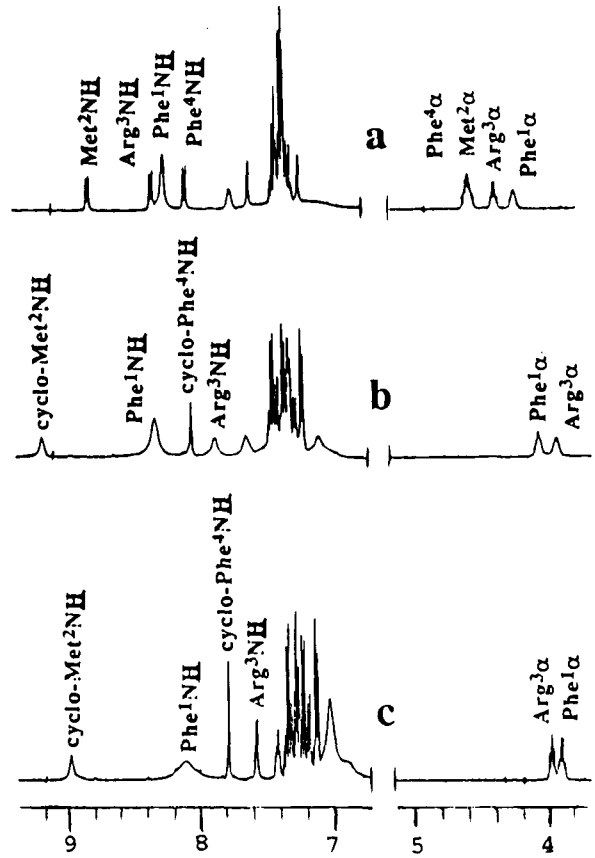


**Figure 8.** $^1$H-NMR spectra for (a) FMRF-$NH_2$ at 25 °C, (b) F{**2*S*,3*S*-cyclo-M**}R{***2R*,3R*-cyclo-F**}-$NH_2$ at 25 °C, and (c) F{**2S,3S-cyclo-M**}R{***2R*,3R*-cyclo-F**}-$NH_2$ at 55 °C.

{***2R*,3R*-cyclo-F**}-$NH_2$ may populate more than one conformational state in DMSO, and equilibration between these is slow on the NMR time scale at 25 °C. Consistent with this, it was observed that the $^1$H-NMR signals for F{**2*S*,3*S*-cyclo-M**}R-{***2R*,3R*-cyclo-F**}-$NH_2$ sharpened considerably as the temperature of the solution was elevated. It seems likely that relatively slow equilibration associated with this molecule was caused by the conformational rigidity imposed by the two cyclopropane rings. The $^1$H-NMR spectrum of F{***2R*,3R*-cyclo-M**}RF-$NH_2$ was not noticeably broadened in this way.

Figure 9 summarizes important features of the NMR spectra collected for the two peptidomimetics. The ROESY spectra of F{**2*S*,3*S*-cyclo-M**}R{***2R*,3R*-cyclo-F**}-$NH_2$ in DMSO showed five interresidue side chain to side chain cross-peaks that were not observed in the corresponding spectrum of FMRF-$NH_2$. The absence of N*H* to N*H* ROE cross-peaks, together with the high temperature coefficients observed for the amide protons (*vide supra*), excluded tight turn structures as major conformers. Three aspects of the NMR data for F{***2R*,3R*-cyclo-M**}RF-$NH_2$ indicate that it has a bias toward a secondary structure that is not observed for FMRF-$NH_2$. First, the chemical shift of the $R^3$N*H* proton was significantly (0.63 ppm) shifted upfield of the corresponding proton in the parent peptide.[19] Second, the **cyclo-$M^2$**-N*H* and $R^3$N*H* protons had temperature coefficients below 3 ppb $K^{-1}$, the cutoff below which a proton is generally assumed to be effected by intramolecular hydrogen bonding or solvent shielding.[35,36] Finally, two interresidue ROE peaks were observed for F{***2R*,3R*-cyclo-M**}RF-$NH_2$ that corresponded to close contacts for the following pairs of protons: ***2R*,3R*-cyclo-M**N*H*-$R^3$N*H* and $F^1$aromatic*H*-***2R*,3R*-cyclo-M**$\beta'_{cis}$.

**Correlation of the NMR and Computational Studies.** Correlations exist between the calculated low-energy structures of F{**2*S*,3*S*-cyclo-M**}R{***2R*,3R*-cyclo-F**}-$NH_2$ and the NMR data for this molecule. Eight ROE cross-peaks corresponding to the backbone and interresidue side chain to side chain ROEs were selected to compare with the representative structures of families for F{**2*S*,3*S*-cyclo-M**}R{***2R*,3R*-cyclo-F**}-$NH_2$ (Table 4). These long-range ROE cross-peaks should better characterize the overall conformation than intraresidue ROEs. The representative structure of family F1 shows a better fit to the ROE data than families F2 to F4. A violation was found for the ***2R*,3R*-cyclo-$F^4$** aromatic*H*-$R^3\gamma$ (a weak ROE was observed, but the calculated distance was >5 Å), and the $Arg^3$N*H*-α connectivity was weaker than expected. However, the proximity of the side chains in the F1 lowest-energy structure (Figure 10) is consistent with the observed side chain to side chain ROEs. It is also reassuring that no hydrogen bond was present in the calculated conformation, and the NMR temperature coefficients for the amide protons indicated that none should be present. Matching the NMR data with all 36 structures within the cutoff provided three structures with interproton distances <5 Å for all of the eight corresponding ROE cross-peaks {Table 4, F1-(22), F1(28), and F1(31)}. All these structures were members of F1, indicating that the F1 type structure agreed well with the solution NMR data (Figure 10).

Table 5 shows that QMD data for the lowest-energy conformer of family F1 for F{***2R*,3R*-cyclo-M**}RF-$NH_2$ accommodated the close contact between ***2R*,3R*-cyclo-$M^2\beta'_{cis}$**-$F^1$-aromatic*H* implicated by the NMR data. However, two discrepancies were found between the NMR data and the F1

(35) Ohnishi, M.; Urry, D. W. *Biochem. Biophys. Res. Commun.* **1969**, *36*, 194.

(36) Ohnishi, M.; Urry, D. W. *Biochem. Biophys. Res. Commun.* **1969**, *36*, 194.

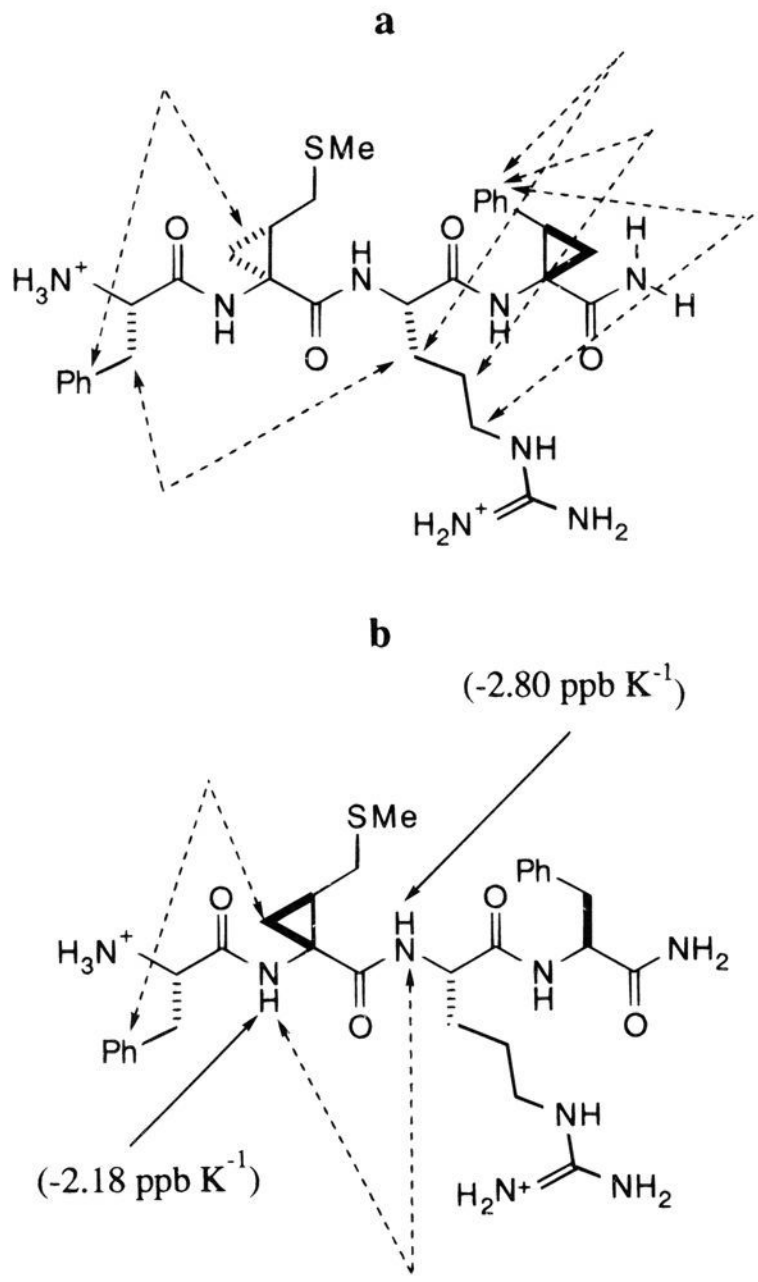


**Figure 9.** Salient NMR data for (a) F{***2S,3S*-cyclo-M**}R{***2R,3R*-cyclo-F**}-$NH_2$ and (b) F{***2R,3R*-cyclo-M**)RF-$NH_2$. ROEs are highlighted with dashed arrows and notable temperature coefficients with solid arrows.

representative structure. First, the interproton distance of 4.21 Å between the **2*R*,3*R*-cyclo-M²**N*H* and $R^3NH$ was too long to generate a medium-intensity cross-peak. Second, there was no obvious structural basis for the low temperature coefficient observed for **2*R*,3*R*-cyclo-M²**N*H* (−2.18 ppb $K^{-1}$); no hydrogen bond was observed for this proton, and hydrophobic shielding was unlikely because the nearest aromatic carbon (one in the $F^1$ aromatic ring) was 4.46 Å from the **2*R*,3*R*-cyclo-M²**N*H* proton.

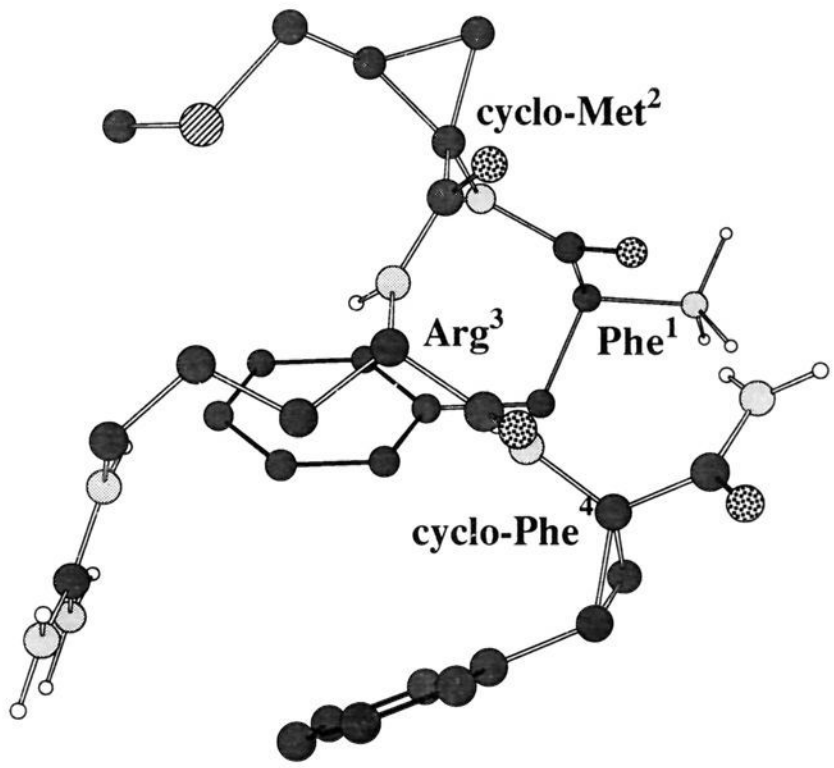


**Figure 10.** Overall lowest-energy conformer (family F1) generated in the QMD study of F{***2S,3S*-cyclo-M**}R{***2R,3R*-cyclo-F**}-$NH_2$.

It was possible to find conformers that did fit the NMR data for F{**2*R*,3*R*-cyclo-M**}RF-$NH_2$ by searching amongst those generated in the QMD study. To do this, the two interresidue ROEs {**2*R*,3*R*-cyclo-M²**N*H*-$R^3NH$ and **2*R*,3*R*-cyclo-M²**$\beta'_{cis}$-$F^1$-aromatic*H*) were used as the selection criteria. These two ROEs were chosen because these were relatively long range, and they were not observed in FMRF-$NH_2$.[19] Constraints of 4 Å (medium) and 5 Å (weak) for **2*R*,3*R*-cyclo-M²**N*H*-$R^3NH$ and **2*R*,3*R*-cyclo-M²**$\beta'_{cis}$-$F^1$aromatic*H*, respectively, were set as the distance cutoffs; hence, conformers with **2*R*,3*R*-cyclo-M²**N*H*-$R^3NH \leq 4$ Å and **2*R*,3*R*-cyclo-M²**$\beta'_{cis}$-$F^1$aromatic*H* ≤ 5 Å were sifted from the pool of 91 conformers within 4 kcal $mol^{-1}$ of the minimum-energy structure. Eight conformers were found to fit these criteria, as shown in Table 6. Six out of the eight adopted negative $\phi$ and negative $\psi$ (average value of $\phi = -71°$ and $\psi = -80°$) for the **2*R*,3*R*-cyclo-M²**, including the lowest energy structure of this group, F1(44). Figure 11 shows the structure of conformer F1(44). The close proximity of the $F^1$ aromatic ring and the **2*R*,3*R*-cyclo-M²**N*H* (the distance of the N*H* to the closest aromatic carbon is 2.75 Å) explains why this particular proton should be shielded from the solvent and would have a low temperature coefficient (−2.18 ppb $K^{-1}$). It seems that the conformers of $\phi \sim -71°$ and $\psi \sim -80°$ at **2*R*,3*R*-cyclo-M²** gave the best fit to the experimental data.

**Table 4.** Qualitative Fit of ROE Cross-Peak Intensities with the Corresponding Interproton Distances for Low-Energy Structures in Each Family and Best-Fit Strucures Generated for F{**2*S*,3*S*-cyclo-M**}R{**2*R*,3*R*-cyclo-F**}-$NH_2$ *via* QMD

| | | distance calculated in the QMD study (Å) | | | | | | |
|---|---|---|---|---|---|---|---|---|
| contact/characteristic | ROE intensity | F1 | F2 | F3 | F4 | F1(22)[a] | F1(28) | F1(31) |
| $Phe^1\alpha$-**2*S*,3*S*-cyclo-Met²**N*H* | S | 2.19 | 2.12 | 3.57 | 3.43 | 2.10 | 2.19 | 2.26 |
| $Arg^3NH$-α | VW | 2.88 | 2.92 | 2.85 | 2.92 | 2.84 | 2.89 | 2.86 |
| **2*R*,3*R*-cyclo-Phe⁴**N*H*-$Arg^3\alpha$ | M | 3.50 | 3.02 | 3.46 | 2.02 | 3.45 | 3.50 | 3.46 |
| $Phe^1$aromatic*H* | W | 4.72 | 3.78 | 3.71 | 4.05 | 4.70 | 4.70 | 4.94 |
| **2*S*,3*S*-cyclo-Met²**$\beta$ and/or $\beta'$ | | | | | | | | |
| $Phe^1\beta$-$Arg^3\beta$s | W | 4.92 | >5.00 | >5.00 | >5.00 | 4.28 | 4.89 | 4.52 |
| **2*R*,3*R*-cyclo-Phe⁴**aromatic*H*$Arg^3\beta$s | VW | 3.72 | >5.00 | >5.00 | >5.00 | 4.00 | 3.71 | 4.13 |
| **2*R*,3*R*-cyclo-Phe⁴**aromatic*H*$Arg^3\gamma$s | W | >5.00 | >5.00 | >5.00 | 3.32 | 3.61 | 3.43 | 3.61 |
| **2*R*,3*R*-cyclo-Phe⁴**aromatic*H*$Arg^3\delta$s | VW | 3.94 | >5.00 | >5.00 | 3.60 | 3.54 | 3.06 | 3.79 |
| $\phi,\psi$ of **2*S*,3*S*-cyclo-Met²** | | −56, −54 | −63, −34 | +81, −34 | +73, −78 | −64, −41 | −54, −55 | −61, −45 |
| $\phi,\psi$ of **2*R*,3*R*-cyclo-Phe⁴** | | −61, −67 | +78, −85 | +74, +80 | +69, +83 | −58, +99 | −61, −72 | −58, −63 |
| number in family | | 8 | 19 | 4 | 2 | – | – | – |
| energy (kcal $mol^{-1}$) | | −11.2 | −9.9 | −8.5 | −8.2 | −8.9 | −7.5 | −9.6 |

[a] Members of F1 and the number represents the identity of the structure.

**Table 5.** Qualitative Fit of ROE Cross-Peak Intensities with the Corresponding Interproton Distances for Low-Energy Structures in Each Family Generated for the QMD Study of F{**2*R*,3*R*-cyclo-M**}RF-$NH_2$ **(2)**

| | | distance calculated in the QMD study (Å) | | | | | |
|---|---|---|---|---|---|---|---|
| contact/characteristic | ROE intensity | F1 | F2 | F3 | F4 | F5 | F6 |
| **2*R*,3*R*-cyclo-Met²**N*H*-Arg3NH | M | 4.21 | 3.79 | 4.20 | 4.02 | 4.16 | 2.94 |
| **2*R*,3*R*-cyclo-Met²**$\beta'_{cis}$-Phe¹aromatic*H* | W | 3.37 | >5.00 | >5.00 | >5.00 | >5.00 | >5.00 |
| **2*R*,3*R*-cyclo-Met²**N*H*-Phe1α | VS | 2.06 | 2.15 | 3.56 | 2.11 | 3.56 | 3.55 |
| Arg³N*H*-α | M | 2.88 | 2.88 | 2.93 | 2.90 | 2.86 | 2.95 |
| Phe⁴N*H*-Arg3α | S | 3.46 | 3.44 | 3.29 | 2.07 | 1.99 | 3.56 |
| Phe⁴N*H*-α | M | 2.90 | 2.89 | 2.90 | 2.92 | 2.90 | 2.95 |
| CONH*H*-Phe⁴α | S | 2.15 | 2.13 | 3.58 | 3.55 | 2.08 | 2.14 |
| $\phi,\psi$ of **2*R*,3*R*-cyclo-Met²** | | +63, −91 | −77, +68 | +67, −94 | −70, +81 | +67, −90 | +53, +46 |
| number in family | | 29 | 4 | 28 | 7 | 7 | 7 |
| energy (kcal $mol^{-1}$) | | −16.4 | -15.4 | −15.0 | −14.9 | −14.6 | −14.3 |

**Table 6.** The Best Qualitative Fit of ROE Cross-Peak Intensities with the Corresponding Interproton Distances in Each Family for the Conformers Generated for F{**2*R*,3*R*-cyclo-M**}RF-$NH_2$ in QMD

| | | distance calculated in the QMD study (Å) | | | | | | | |
|---|---|---|---|---|---|---|---|---|---|
| contact/characteristic | ROE intensity | F1(44)[a] | F5(88) | F1(65) | F2(51) | F2(1) | F1(91) | F1(42) | F1(45) |
| **2*R*,3*R*-cyclo-Met²**N*H*-Arg³N*H* | M | 2.86 | 3.51 | 2.91 | 2.81 | 2.68 | 3.03 | 3.04 | 2.91 |
| **2*R*,3*R*-cyclo-Met²**$\beta'_{cis}$-Phe¹aromatic*H* | W | 3.21 | 4.99 | 3.09 | 2.83 | 3.17 | 4.62 | 3.74 | 3.02 |
| **2*R*,3*R*-cyclo-Met²**N*H*-Phe¹α | VS | 3.53 | 2.14 | 3.54 | 3.55 | 2.13 | 2.14 | 3.52 | 3.54 |
| Arg³N*H*-α | M | 2.84 | 2.92 | 2.86 | 2.89 | 2.92 | 2.82 | 2.85 | 2.85 |
| Phe⁴N*H*-Arg³α | S | 3.48 | 2.02 | 3.53 | 3.51 | 3.35 | 3.53 | 3.45 | 3.43 |
| Phe⁴N*H*-α | M | 2.91 | 2.88 | 2.93 | 2.94 | 2.89 | 2.95 | 2.90 | 2.90 |
| CONH*H*-Phe⁴α | S | 2.11 | 2.08 | 3.38 | 3.49 | 3.50 | 3.49 | 3.50 | 3.56 |
| $\phi,\psi$ of **2*R*,3*R*-cyclo-Met²** | | −71, −70 | −71, −102 | −79, −80 | −84, +18 | +63, +47 | −60, −72 | −71, −78 | −76, −76 |
| energy (kcal $mol^{-1}$) | | −15.1 | −14.4 | −14.0 | −13.4 | −13.0 | −12.6 | −12.3 | −12.2 |

[a] The number represents the identity of the structure in the corresponding family.

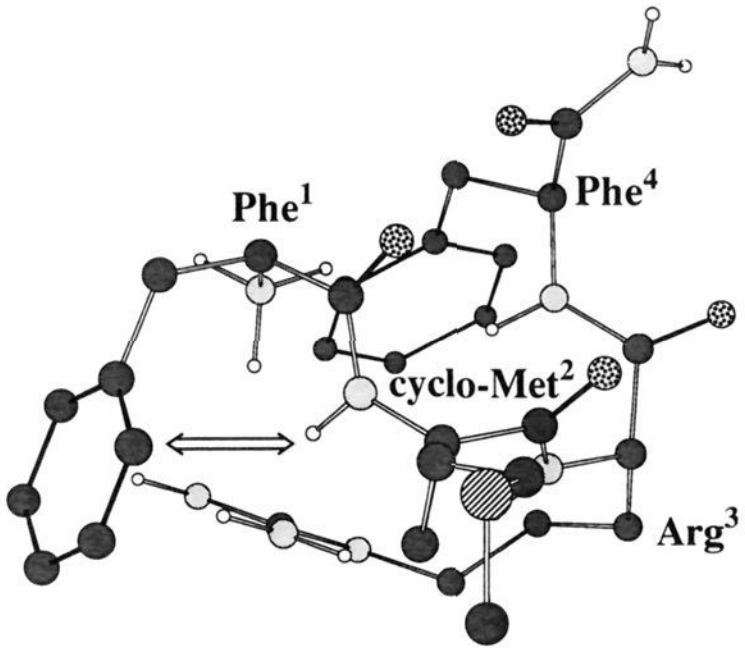


**Figure 11.** Lowest-energy conformer {F1(44)} of the eight best-fit conformers for F{**2*R*,3*R*-cyclo-M**}RF-$NH_2$ chosen on the basis of distance constraints. The double arrow is intended to indicate close proximity between the $F^1$ aromatic ring and the **2*R*,3*R*-cyclo-M²**N*H*.

## Conclusions

Dot plots of $\phi,\psi$ angles derived from QMD studies provide a good format with which to visualize the fundamental conformational effects of 2,3-methanoamino acids. These conformational effects are dependent on the stereochemistry of the molecule used. *Cis* 3-substituted methanoamino acids have severely restricted $\phi$ torsions, but $\psi$ angles are more constrained for *trans* derivatives. Enantiomers of *cis* 3-substituted methanoamino acids have different preferred $\phi$ values, *i.e.* more negative or more positive, depending on the stereochemistry.

Local effects of 2,3-methanoamino acids are more easily rationalized than the secondary structures adopted by the peptidomimetics containing them. This is not surprising when this situation is compared with the currently insurmountable difficulties associated with predicting peptide conformations from sequence data. However, 2,3-methanoamino acids are more constrained than the natural protein amino acids so the problems associated with determining secondary structures of peptidomimetics containing them are less formidable.

Replacing the $F^4$ of F{**2*S*,3*S*-cyclo-M**}RF-$NH_2$ with **2*R*,3*R*-cyclo-F** (*i.e.* F{**2*S*,3*S*-cyclo-M**}R{**2*R*,3*R*-cyclo-F**}-$NH_2$) destroyed the bias toward a $\gamma$-turn structure centered at the **2*S*,3*S*-cyclo-M²** residue.[19] In the calculated preferred structures, the two peptidomimetics adopted $\phi,\psi$ values about the same 2,3-methanoamino acid (**2*S*,3*S*-cyclo-M²**) of approximately 64, −82° and −60, −45°, respectively. The only difference between them is that between F and **2*R*,3*R*-cyclo-F** at position 4, so these observations illustrate the strong effects that peripheral amino acids can have on the secondary structure of peptidomimetics, even with respect to the same conformationally constrained amino acid residue.

Apparently the match of the conformational bias of the peptide backbone with the local effects for F{**2*R*,3*R*-cyclo-M**}-RF-$NH_2$ is not so good as for the peptidomimetics containing the enantiomeric methanolog F{**2*S*,3*S*-cyclo-M**}RF-$NH_2$. The former has more conformational rigidity than FMRF-$NH_2$, with conformations having $\phi \sim -71°$ and $\psi \sim -80°$ at the **2*R*,3*R*-cyclo-M²** residue being preferred, but there is no clear preference for any readily identified element of secondary structure. From the QMD simulations, it appears that several conformations of this peptidomimetic are close to the global minimum; hence, correlations between the calculated preferred conformations and the NMR data are relatively poor. Another reason for this discrepancy may also be the use of a dielectric of 45 to represent DMSO. This simplification is drastic and may be inadequate in this particular case.

**Acknowledgment.** We thank Dr. B. M. Pettitt for introducing us to the QMD technique and for some helpful suggestions. We also thank Chun-Yen Ke, Wen Li, and Dongyeol Lim for

reading the manuscript. K.B. acknowledges support from NIH and The Robert A. Welch Foundation. K.B. also thanks the NIH for a Research Career Development Award and the Alfred P. Sloan Foundation for a fellowship. We would like to thank Mr. S. Silber for helpful discussions concerning NMR.

**Supplementary Material Available:** One-dimensional $^1$H-NMR, DQF-COSY, and ROESY spectra for F{**2*S*,3*S*-cyclo-M**}R{**2*R*,3*R*-cyclo-F**}-$NH_2$ and for F{**2*R*,3*R*-cyclo-M**}RF-$NH_2$. CHARMM topology and parameter file for **2*R*,3*R*-cyclo-F**, **2*S*,3*S*-cyclo-M**, and **2*R*,3*R*-cyclo-M** (10 pages). This material is contained in many libraries on microfiche, immediately follows this article in the microfilm version of the journal, can be ordered from the ACS, and can be downloaded from the Internet; see any current masthead page for ordering information and Internet access instructions.

JA942647N